Article

Coevolution of craton margins and interiors during continental break-up

https://doi.org/10.1038/s41586-024-07717-1

Received: 25 March 2022

Accepted: 13 June 2024

Published online: 7 August 2024

Open access

Check for updates

Thomas M. Gernon[1]✉, Thea K. Hincks[1], Sascha Brune[2,3], Jean Braun[2,3], Stephen M. Jones[4], Derek Keir[1,5], Alice Cunningham[1] & Anne Glerum[2]

Many cratonic continental fragments dispersed during the rifting and break-up of Gondwana are bound by steep topographic landforms known as 'great escarpments'[1–4], which rim elevated plateaus in the craton interior[5,6]. In terms of formation, escarpments and plateaus are traditionally considered distinct owing to their spatial separation, occasionally spanning more than a thousand kilometres. Here we integrate geological observations, statistical analysis, geodynamic simulations and landscape-evolution models to develop a physical model that mechanistically links both phenomena to continental rifting. Escarpments primarily initiate at rift-border faults and slowly retreat at about 1 km Myr^{-1} through headward erosion. Simultaneously, rifting generates convective instabilities in the mantle[7–10] that migrate cratonward at a faster rate of about 15–20 km Myr^{-1} along the lithospheric root, progressively removing cratonic keels[11], driving isostatic uplift of craton interiors and forming a stable, elevated plateau. This process forces a synchronized wave of denudation, documented in thermochronology studies, which persists for tens of millions of years and migrates across the craton at a comparable or slower pace. We interpret the observed sequence of rifting, escarpment formation and exhumation of craton interiors as an evolving record of geodynamic mantle processes tied to continental break-up, upending the prevailing notion of cratons as geologically stable terrains.

Cratons experience extremely low erosion rates when viewed over geological time[12], a feature attributed to their mechanical strength and prolonged stability[13,14]. Thus, the formation of great escarpments (hereafter, escarpments) (Fig. 1) and subsequent uplift of craton interiors are geologically abrupt and enigmatic[15] events that disrupt[6] this long-term stability. Escarpments, that is, laterally extensive breaks in slope about a kilometre high and many thousands of kilometres long, typically occur near the edges of shields—tectonically stable regions rooted on strong cratons[16] (for example, Eastern Brazil, Southern Africa and the Western Ghats of India; Fig. 1a–c). Although a widely held view is that these landforms originate during continental rifting[2–4,17–19], the mechanistic linkages are not well resolved.

Escarpments have been attributed to various processes, including: (1) flexurally induced uplift along rift flanks owing to lithospheric unloading during extension[2,20–22]; (2) small-scale convection induced by lateral temperature gradients, driving uplift of rift shoulders[7,8]; and (3) downgrading of the coastal area and inland base-level fall[23]. Crucially, the relationship of these processes to anomalous exhumation that occurs in remote hinterland plateau regions long after rift termination[5,18,24,25] is poorly understood. Flexural uplift is typically confined to the rift flanks and cannot explain the formation of an elevated continental interior. Studies have variously invoked prolonged plateau uplift[26–29] (for example, through compression-induced uplift unrelated to rifting and break-up[28]), post-rift tectonic reactivation[29–31] and passive-margin rejuvenation[17]. However, whether the last process occurs is disputed[3].

Surface processes occurring far from rift zones[5,18,24,25,29] (>500 km away) and long (tens of millions of years) after rift cessation seemingly prohibit a first-order role for rifting. Several studies, such as for the classic Great Escarpment of South Africa (Fig. 1d–f), instead propose that plate movement over a large, low-shear-velocity province, exposing the continent to deep, buoyant mantle upwelling, drives rapid uplift and surface erosion over a broader region[32]. However, such a superswell is not observed in dynamic support histories derived from diverse continental and oceanic records[33]. Further, evidence for protracted plateau uplift since escarpment formation[18] contradicts the notion of post-break-up tectonic stability proposed by the downgrading model[23]. Alternatively, enduring surface uplift surrounding the escarpment might reflect intermediate-scale (approximately 1,000 km) present-day mantle convective support[16,22,32–34], possibly associated with cratonic-edge-driven convection[17,35]. Stochastic inversion models indicate that dynamic mantle support contributes approximately 650 m to the regional elevation in Southern Africa, with the remaining elevation (about 670 m) attributed to the isostatic lithospheric contribution[34]. This estimate is supported by independent modelling studies that suggest up to 1 km of dynamic/static mantle support[15].

[1]School of Ocean & Earth Science, University of Southampton, Southampton, UK. [2]Helmholtz Centre Potsdam – GFZ German Research Centre for Geosciences, Potsdam, Germany. [3]University of Potsdam, Potsdam, Germany. [4]School of Geography, Earth and Environmental Sciences, University of Birmingham, Birmingham, UK. [5]Dipartimento di Scienze della Terra, Universita degli Studi di Firenze, Florence, Italy. ✉e-mail: T.M.Gernon@soton.ac.uk

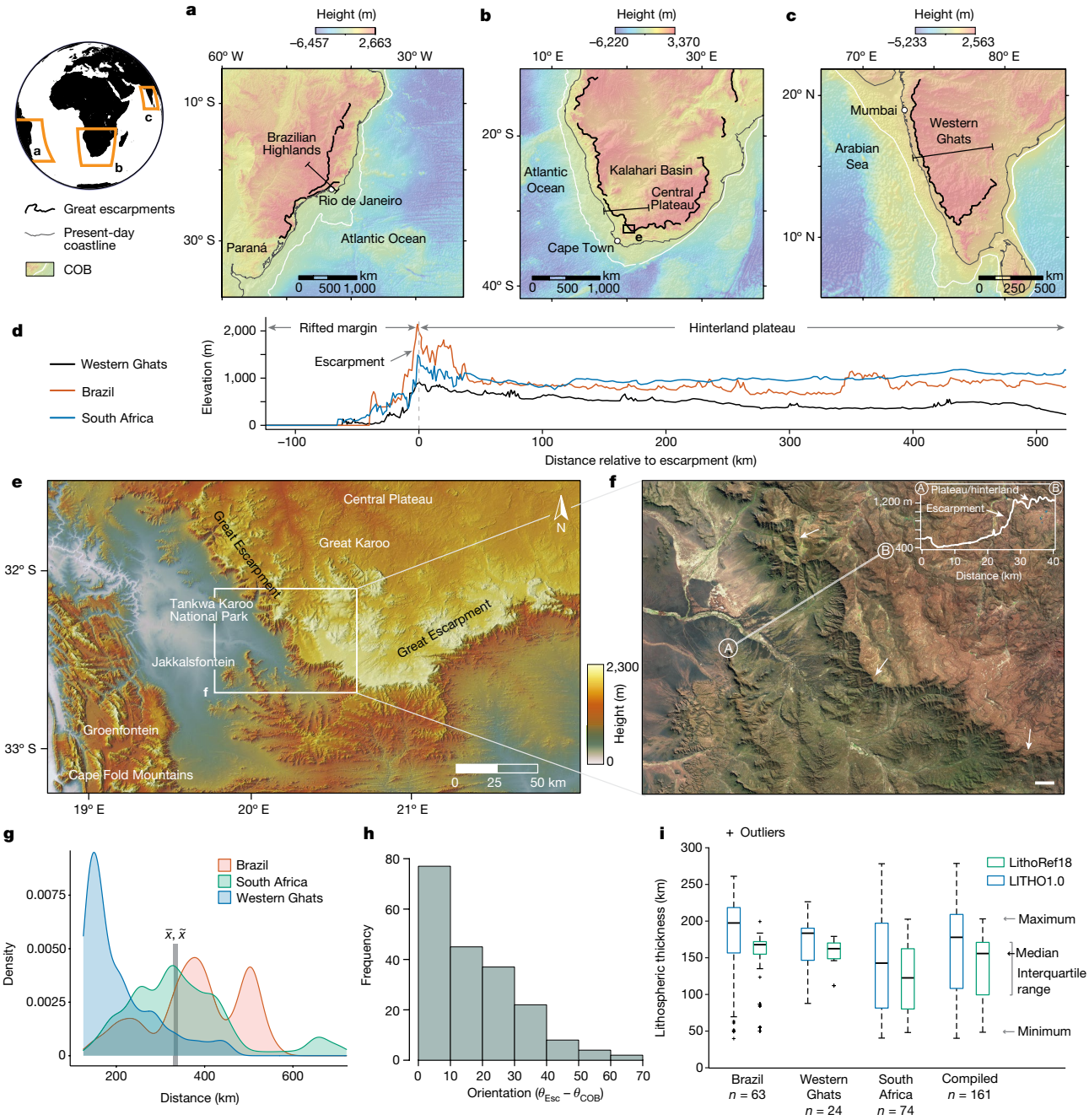

Fig. 1 | Location and physical characteristics of great escarpments. Global terrain maps for ocean and land (gridded data from GEBCO) of the east coast of Brazil (**a**), Southern Africa (**b**) and the Western Ghats (Sahyadri Hills), India (**c**) (see inset map for locations). The maps show a simplified representation of escarpments mapped using digital terrain models (Methods) and COBs from GPlates[59] (https://www.gplates.org/). **d**, Topographic profiles of escarpments (see **a**–**c** for lines of section). **e**, Map of the Great Escarpment of South Africa (see **b** for location) generated using NASA SRTM elevation data (Lambert conformal conic projection). **f**, Short-wave infrared satellite image of the same escarpment (white arrows) from Sentinel Hub. A typical topographic profile is shown (A–B). Sinuosity of escarpments is related to contrasted retreat rates of channels relative to interfluves[1]. Scale bar, 5 km. **g**, Probability density for nearest distance between escarpments and COBs for the regions (see **a**–**c**). Global mean and median thicknesses (vertical grey band) are 336 and 333 km, respectively (n = 5,288; Extended Data Fig. 3a–c). Two distinct peaks for Brazil reflect two phases of escarpment formation there (Cretaceous and Cenozoic)[3]. **h**, Difference in orientation between escarpments (θ_{Esc}) and COBs (θ_{COB}) calculated using the perpendicular to the escarpment tangent at 50-km intervals (n = 195; Methods and Extended Data Fig. 2). Escarpments are typically sub-parallel to adjacent COBs (Extended Data Fig. 3d–g). **i**, Box plot of lithospheric thickness for each escarpment, point sampled from maps generated using LITHO1.0 (ref. 41) (blue boxes) and LithoRef18 (ref. 42) (green boxes) at 1.0°, or approximately 111-km, intervals (n = 161).

Drawing from the above examples, the broader context of landform formation following continental break-up is heavily debated. This study aims to quantify the spatial and temporal relationships between rift systems and the generation of escarpments and plateaus, while using geodynamic and landscape-evolution modelling to gain a quantitative understanding of the mechanisms influencing these regions.

Origin of great escarpments

We begin by evaluating the physical characteristics of escarpments and examining their spatial and temporal relationships to continental margins and high-elevation hinterland plateaus. First, we focus on the main coastal escarpments, associated with cratonic lithosphere, which formed between 150 and 70 million years ago (Ma) during the break-up of Gondwana (Extended Data Fig. 1). We compare three classic coastal escarpments in Southern Africa, Brazil and the Western Ghats, spanning distances of approximately 6,000, 3,000 and 2,000 km, respectively (Fig. 1a–c). These length scales allow us to analyse their lithospheric properties using global reference models with low resolution (100–200 km). Older escarpments in northwest Africa and the eastern USA, associated with protracted rifting and break-up of cratonic lithosphere in the Central Atlantic (between approximately 240 and 180 Ma), feature more subdued topography shaped by prolonged post-rift erosion[22] and are not a direct focus of our study.

Given their spatial and topographic characteristics, it is plausible that escarpments initiate as rift-border faults such as those kilometre-high escarpments separating the high-elevation Ethiopian Plateau from the East African Rift today[36]. In that case, their orientation and spacing with respect to continent–ocean boundaries (COBs), delineating ancient rift axes, should be broadly similar and closely mimic those generated in numerical models[19]. To examine this, we map the escarpments in detail (Fig. 1a–d) using geoprocessing tools in the ArcGIS software package. We then analyse the first-order spatial and topological attributes of escarpments and COBs (Fig. 1d and Extended Data Fig. 2) using the statistical computing package, R (https://www.r-project.org/; see Methods).

The mean distance between escarpments and COBs varies across different regions, ranging from 207 km in the Western Ghats to 380 km in Brazil (Fig. 1g and Extended Data Fig. 3g). Global mean and median distances range from 330 to 340 km (Fig. 1g and Extended Data Fig. 3g). When we compare the orientations of geographic domains of escarpments to the adjacent sections of COBs (Methods), we find that they are sub-parallel over scales ranging from 10^2 to 10^3 km (Fig. 1h). These data suggest that escarpments originate at or near border faults, that is, at the inner boundary of rifted continental margins. Indeed, the distance between escarpments and the nearest oceanic crust (that is, outer boundary of the rifted margin) is similar to the estimated half-width of rift zones in the studied regions, which fall in the range 250–600 km (ref. 37). The mean distances between escarpments and COBs (Fig. 1g) closely align with predictions from numerical models[19] and support rifting as a driver of escarpment formation[2–4].

Rifting alone cannot satisfactorily explain the broad uplift and denudation patterns in hinterland regions, in which further scarp retreat occurred in the Cretaceous[5,18,24,25]. It is feasible that marginal uplift is more pronounced where the cratonic lithosphere is thick and underlain by a weak, basal layer that undergoes convective removal or delamination—a process that gives rise to isostatic uplift[38,39]. Since such processes are not expected to substantially thin the lithosphere (that is, more than about 35 km)[11,40], the present-day lithospheric thickness offers a rough guide to that in the recent geological past. To investigate lithospheric-thickness characteristics along our coastal escarpments (Fig. 1a–c), we sample this property using two different global reference models—LITHO1.0 (ref. 41) and LithoRef18 (ref. 42)—at regular 1.0° intervals (commensurate with model resolution; Methods). Although locally variable, the escarpments generally occur on thick lithosphere, that is, the lithosphere–asthenosphere boundary (LAB) occurs at a median depth of 177 km or 155 km (Fig. 1i) for the two global reference models, respectively.

The escarpments form primarily near the boundaries of continental lithosphere along rift-border faults (Fig. 1). Their sustained elevation is because of a combination of factors, including lithospheric thickness (Fig. 1i), flexural uplift[2,20,21], mantle convection[7,8] and dynamic mantle support[16,32–34]. Escarpments climb into higher terrain through headward erosion, causing them to retreat further inland[21]. This rapid retreat stops on reaching a point at which it functions as a pinned drainage divide, that is, a fixed boundary between drainage basins. For example, in response to tectonic uplift, the westward-draining Karoo River of South Africa (proto-Orange River; Extended Data Fig. 4a) incised a deep channel through the Great Escarpment[43] at 120–110 Ma (refs. 29,43), paving the way for fluvial erosion of the hinterland plateau[44]. Because eroded sediments are largely transported westward into the Orange Basin, this phase of onshore denudation—a west-to-east 'wave' of erosion[44]—is recorded as a step increase in sediment accumulation rates in marine archives[29,45,46]. Drainage systems, which shaped plateau evolution, may have fundamentally responded to mantle processes (for example, delamination)[5,11,25,40,47] following break-up. However, the nature of these geodynamic processes and their connections to geomorphology remain poorly understood.

Modelling mantle–surface connections

Considering this gap, we investigate the influence of rifting and mantle dynamics on regional exhumation patterns. We use numerical thermomechanical simulations, building on our earlier work[11] and applying conditions and material properties deemed reasonable within the context of previous geodynamic studies (Methods and Extended Data Table 1). Our simulations show that Rayleigh–Taylor (convective) instabilities[9,10], with characteristic wavelengths of about 50–100 km, form at lithospheric edges beneath the rift[11]. The simulations show that instabilities are initiated by: (1) upward suction of low-viscosity mantle beneath the rifting lithosphere, causing the first delamination event (Fig. 2a); (2) formation of a lithospheric edge during continental necking, inducing lateral temperature and viscosity gradients that generate edge-driven convection cells (Fig. 2c); and (3) sequential delamination (Fig. 2c–g), which combines with (2) to produce complex, edge-driven convection patterns. Delamination exploits the density and strength contrast between the colder lithosphere and hotter asthenosphere across the thermal boundary layer (TBL)[11]. Instabilities migrate cratonward at a rate of 15–20 km Myr^{-1}, sequentially removing the TBL to drive adiabatic upwelling of asthenosphere and kimberlite volcanism[11] (Fig. 2).

Although our reference model is 300 km deep and is pulled on one side only (Fig. 2), we further assessed the impact of symmetric boundary conditions, different extension velocities (5 and 20 mm $year^{-1}$ instead of 10 mm $year^{-1}$) and the vertical extent of the model domain (to 410 km; Methods and Extended Data Fig. 5). In all scenarios, the process of sequential delamination occurs as in the reference model, with no marked change in instability spacing (Supplementary Videos 1–4). Migration rates differ only slightly from the reference model (that is, 11 to 15 km Myr^{-1} for the symmetric model) and are in full agreement with observational constraints.

We next ask how much crustal exhumation could realistically be driven by lithospheric removal. Our simulations imply that the lithospheric keel is removed rapidly over distances of hundreds of kilometres parallel to the continental break-up boundary (Fig. 2). The area of removed keel subsequently propagates hundreds of kilometres inland of the break-up zone. Thus, the footprint of the region in which the lithosphere has been thinned by removing its keel is much greater than the elastic thickness of the lithosphere. Therefore, we can use a simple Airy isostatic case to estimate the magnitudes of surface uplift and erosion. Rapid thinning of the lithosphere causes initial uplift at Earth's surface of:

$$s = b\frac{\Delta\rho}{\rho_a} \quad (1)$$

in which b is the thickness of the lithospheric keel that has been removed, ρ_a is the density of the asthenosphere and $\Delta\rho$ is the mean density difference between the lithospheric keel and the asthenosphere

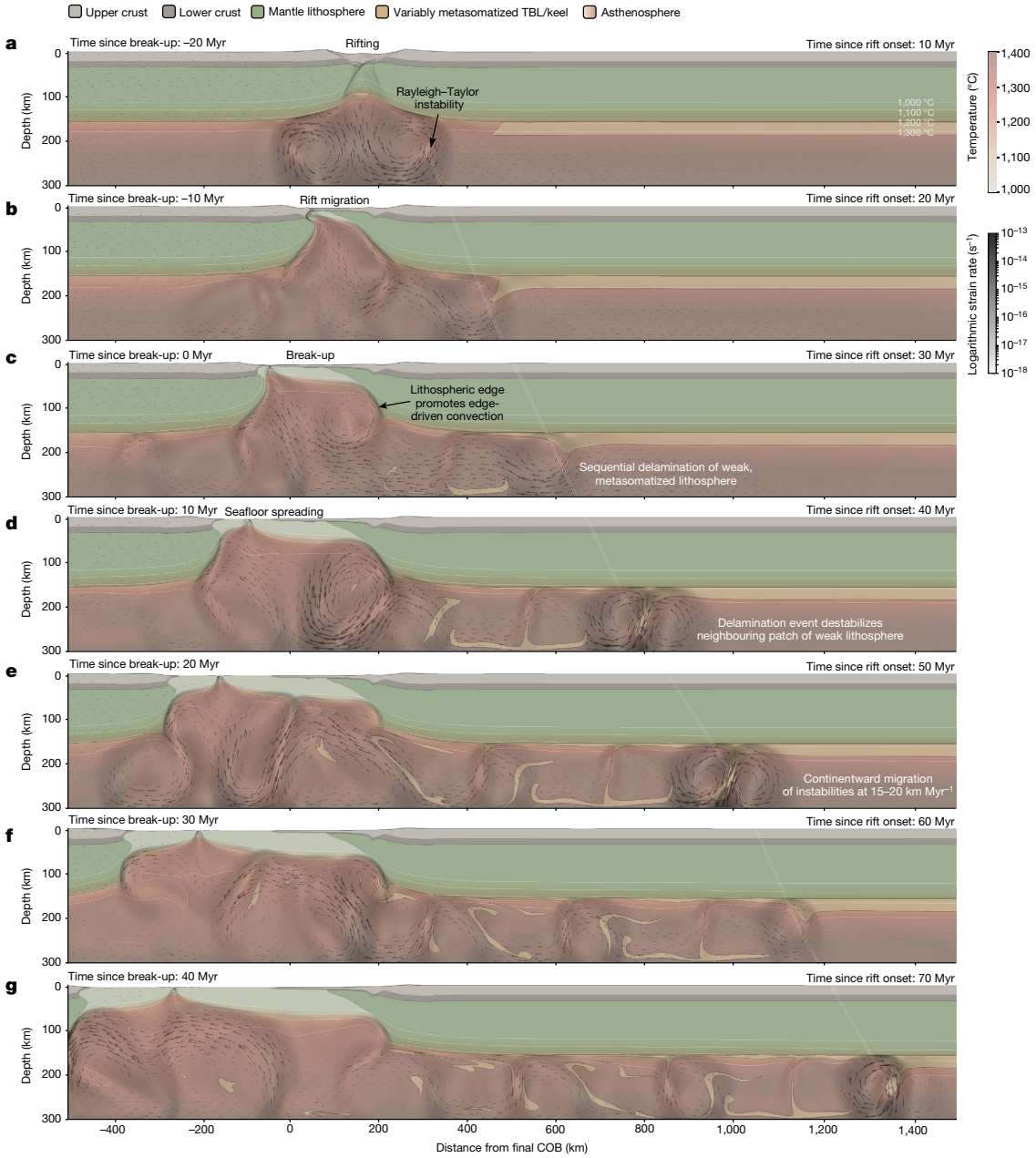

Fig. 2 | Geodynamic models of rift evolution. a–g, The sequential migration of Rayleigh–Taylor instabilities along the lithospheric keel, causing convective removal of the TBL (beige). This process, migrating at a rate of 15–20 km Myr^{-1}, drives a 'wave' of isostatic uplift and surface denudation that similarly migrates across the craton at a comparable rate, and in some cases, more slowly, reflecting delayed landscape response times. The spatial and temporal extent of this process is limited by the width of the continent. Rift onset occurs 10 Myr before the time step shown in **a**, with continental break-up and seafloor spreading occurring in time steps **c** and **d**, respectively. Note that the reference frame is chosen such that the right continent is fixed, whereas the left continent is moving at 10 mm year^{-1}. Values provided above each image on the left-hand side show timing relative to continental break-up in panel **c**. The images are adapted from ref. 11, which provides the animation for this reference model. In the simulations (see Supplementary Videos 1–4), the rift-border fault, or proto-escarpment, is 100–300 km from the COB.

(not to be confused with the density difference between the asthenosphere and the crust; see Extended Data Fig. 6 for a schematic).

It is well established that uplift drives intensified surface erosion[38], leading to further isostatic rebound. For the endmember case in which the new surface uplift is eroded back to the original base level, the total amount of denudation is given by:

$$d = s\frac{\rho_a}{\rho_a - \rho_c} \quad (2)$$

in which ρ_c is the density of the eroded crust (Extended Data Table 2). Combining these two expressions gives the maximum amount of denudation in terms of the thickness of lithospheric keel removed:

$$d = b\frac{\Delta\rho}{\rho_a - \rho_c} \quad (3)$$

Using indicative density values (Extended Data Table 2), the isostatic factor relating lithospheric keel thickness to initial surface uplift

(equation (1)) is 0.003. The isostatic factor that relates initial uplift to maximum denudation (equation (3)) is 0.03–0.04; that is, the total erosion can be about an order of magnitude greater than the initial uplift. If the entire lithospheric TBL is removed, equivalent to removing an approximately 35-km-thick keel[11], the initial uplift (equation (1)) will be about 50–100 m. This uplift can then be amplified by erosion (equation (3)), resulting in total denudation of approximately 0.8 km but, sampling for a range of variables (equations (1)–(3); Extended Data Table 2), plausibly lies in the range 0.5–1.6 km (Extended Data Fig. 7). Combining insights derived from our geodynamic simulations and analytical models, we anticipate that cratonic exhumation on a kilometre-scale should occur in the several tens of millions of years after break-up, and crucially, that the locus of denudation should progressively migrate inboard of escarpments over time (Fig. 2). Both predictions can be tested using surface-process constraints.

Constraints from thermochronology

To examine the exhumation histories of cratons, we turn to thermochronology. Although much work has focused on escarpment retreat rates, which are relatively low (roughly 1 km Myr^{-1})[21], we are primarily concerned with the long-wavelength patterns (covering distances of 10^2–10^3 km) of exhumation across cratons. We first compile published thermal history models, mainly from apatite (U–Th)/He (AHe) and apatite fission track (AFT) analyses (Extended Data Table 3) spanning a classic intracratonic region, the Central Plateau of South Africa[5,14,25,31,44,48–50] (Fig. 1b and Extended Data Fig. 4). Many of these careful measurements were collected by Stanley et al.[5,25,44], who compiled AFT and AHe ages for the region[18] and documented a major phase of Cretaceous cooling across Southern Africa. The thermochronology data used in the original models, mostly derived in previous studies using the inverse modelling software HeFTy[51], can potentially be reconciled by a field of viable time–temperature (t–T) paths. To estimate the most probable timing of cooling and evaluate uncertainties across 47 plateau sites, we use published best-fit t–T paths, upper and lower envelopes encompassing time uncertainty and individual model thermochronology curves (Extended Data Table 3). This information allows us to estimate the total temperature drop (°C), maximum rate of temperature drop (max(dT/dt), measured in °C Myr^{-1}) and its corresponding timing ($t_{\max\frac{dT}{dt}}$), along with associated model uncertainties. We assess max(dT/dt) over a 2-Myr symmetric (rectangular) moving window (see Methods).

Our analysis confirms a protracted history of exhumation, with an acceleration in cooling between 120 and 110 Ma (Extended Data Fig. 8a), as recognized in previous studies[5,25]. This phase of exhumation coincides with a step change in kimberlite petrogenesis probably related to lithospheric removal[11,47]. In this region, denudation rates may have peaked at 175 m Myr^{-1} during the Cretaceous[48]. Such rates are anomalously high when viewed in the context of long-term cratonic erosion rates (about 2.5 m Myr^{-1}) and high even with respect to young, high mountain belts[12], making them difficult to explain in the absence of mantle forcing. The erosion was probably driven by an isostatic response to partial removal of lithospheric mantle[11,47], supported by geochemical evidence for lithospheric delamination from deep kimberlite-hosted xenoliths[11,14,40,47]. Indeed, geothermometry of kimberlite xenoliths from the Kaapvaal Craton of South Africa indicate that upper-mantle temperatures were approximately 100 °C hotter after 100 Ma (ref. 47), pointing to profound thermal, chemical and petrological modification of cratonic lithosphere at this time[11,40,52].

Although a component of the modelled cooling could be post-magmatic (that is, directly related to kimberlite volcanism), magmatic cooling is expected to be rapid (<10 kyr), in contrast to the longer-wavelength cooling trends observed (typically >2 Myr; Methods). Nevertheless, we evaluate this possibility by performing further modelling that conservatively removes all cooling spatiotemporally associated with kimberlites (Methods). This analysis confirms that magmatism can theoretically only explain a very small portion of the broad cooling trend observed over time (Extended Data Fig. 8a). The first-order trends are more consistent with denudation, as suggested previously[48].

Focusing on the Central Plateau, in which thermochronological data coverage is extensive (Extended Data Fig. 4), we examine spatial changes in exhumation through time (Fig. 3). Abrupt exhumation

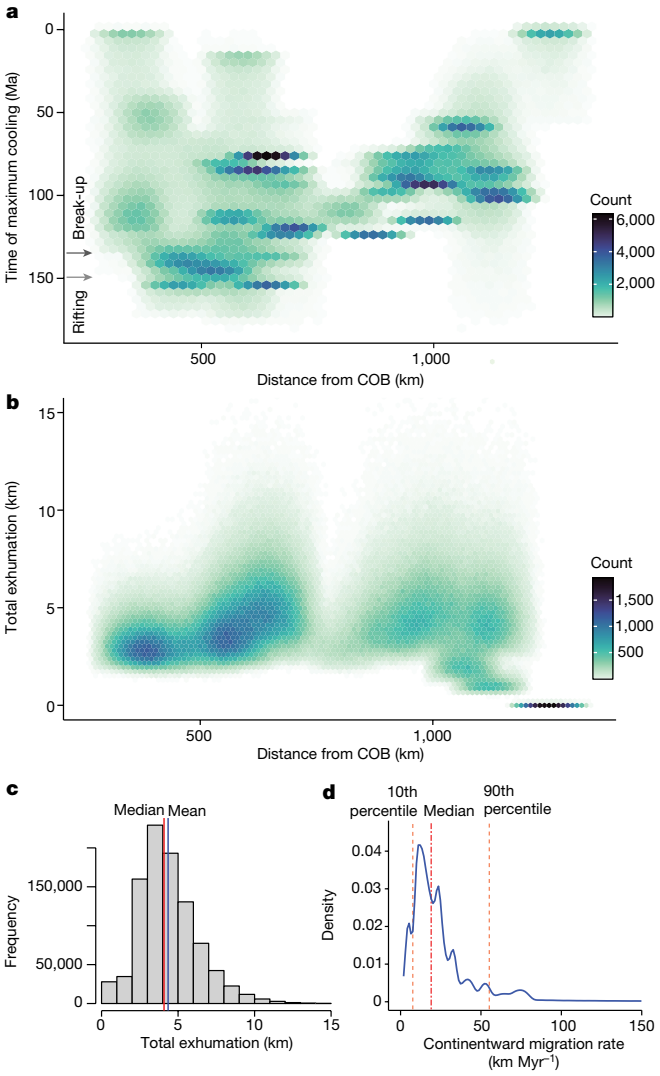

Fig. 3 | Exhumation of the Central Plateau of Southern Africa through time. **a**, Hexagonal heat map showing the statistically defined times of maximum temperature drop ($t_{\max\frac{dT}{dt}}$) from thermochronology at 47 sites across the plateau (Extended Data Table 3). This plot was generated using Monte Carlo sampling (20,000 samples per site) of the estimated time and distance uncertainty at each site (see Methods and Extended Data Fig. 8b). **b**, Hexagonal heat map showing the estimated total exhumation for each site (47 sites, 20,000 samples per site) from 180 to 0 Ma using best-fit thermal history models and accounting for uncertainties in distance and geothermal gradient (see Methods and Extended Data Fig. 8c). **c**, Histogram of sampled total exhumation (n = 940,000), with mean and median values of 4.35 and 4.06 km, respectively. **d**, Density plot showing the apparent continentward migration rates of maximum cooling at thermochronology sites (n = 784,659 samples, or 87% out of 940,000; that is, post-break-up cases only) relative to the timing of continental break-up at the South Atlantic COB (135 Ma)[54]. The median rate is 19.1 km Myr^{-1} and the 10th and 90th percentiles are 7.7 and 55.2 km Myr^{-1}, respectively.

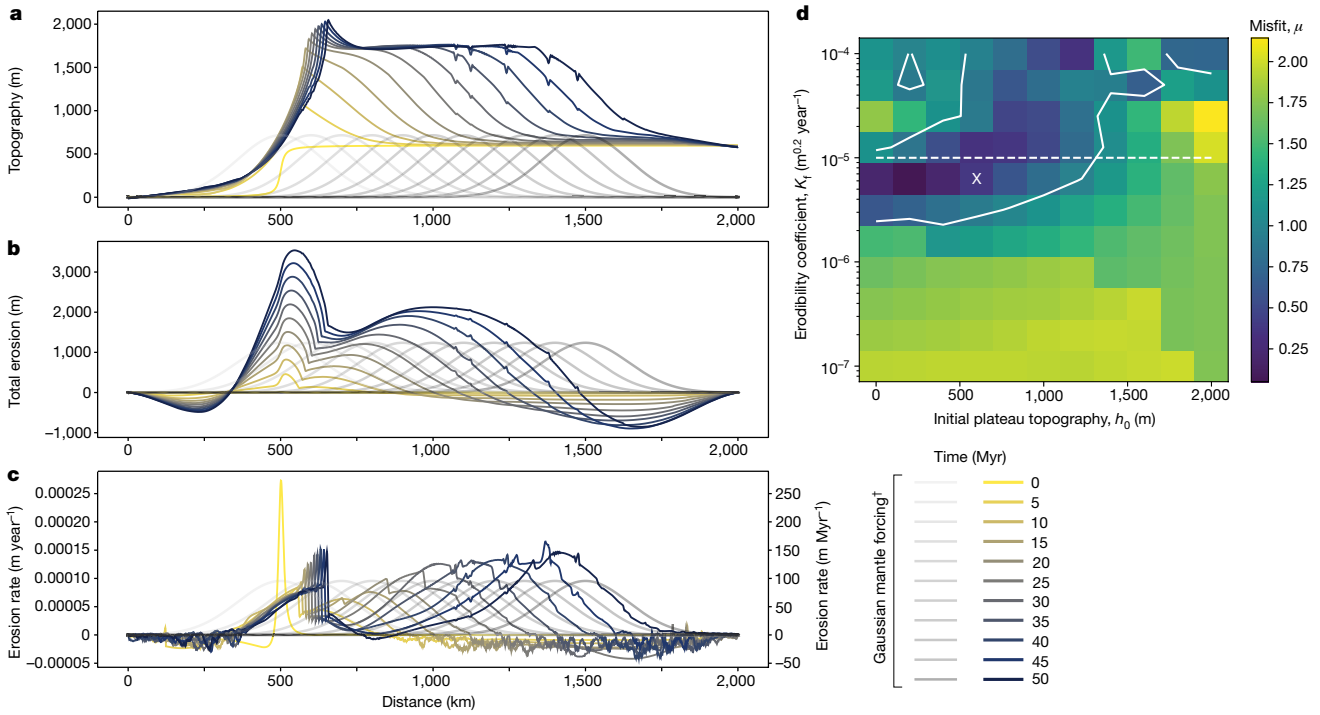

Fig. 4 | Landscape-evolution model. Model results showing the evolution of topography (**a**), total erosion (**b**) and erosion rate (**c**) over a period of 50 Myr following initial escarpment formation (Methods). Note how the escarpment becomes a pinned drainage divide, yet the broad locus of erosion migrates inboard in response to dynamic mantle (Fig. 2) forcing represented by the grey Gaussian curves (†*y*-axis scale not shown because of variations in the maximum uplift rate across model runs, which depends on the other parameters, namely, wave width, velocity, relative densities and initial topography; see Methods). **d**, Plot of the misfit function (μ) calculated by assuming optimum plateau height, denudation and final position of the drainage divide (Methods). Note that a misfit value < 1 means that these conditions are met and white contours indicate where this is true. 'X' denotes the position of the model (in parameter space) shown in **a**–**c**. Dashed line denotes the maximum limit of acceptable values for K_f that would allow the plateau to survive to the present day.

started near the South Atlantic margins during Upper Jurassic to Lower Cretaceous rifting[29,44,50,53] and progressed eastward (Extended Data Fig. 4b), perhaps reflecting erosional scarp retreat processes[5,24,44] (distinct from the earlier Great Escarpment that remained fixed near the plateau edge; Fig. 1). To further investigate this migration pattern, we analyse the timing of maximum cooling, $t_{\max\frac{dT}{dt}}$, across the plateau in relation to the distance from the South Atlantic rifted margins[54]. We find that, in general, the locus of uplift and denudation migrates inboard of continental margins after break-up (Fig. 3a and Extended Data Fig. 8b) and does so at a median rate of 19.1 km Myr^{-1} (Fig. 3d), overlapping with the migration rates of convective instabilities in our simulations (Fig. 2) and kimberlite volcanism[11]. This trend is consistent with a progressive decrease in AHe ages (using data from ref. 18) towards the east of the plateau (Extended Data Fig. 9).

Our analysis of thermal history models for Southern Africa[5,25,31,44,48,50,53,55] indicates that the greatest plateau exhumation, averaging around 4 km in total since 180 Ma (sampling for uncertainty in geothermal gradients; Fig. 3b,c and Extended Data Figs. 4c and 8c), occurs for tens of millions of years after break-up, consistent with offshore sediment accumulation records[18,45,48]. In Southern Namibia, the escarpment and interior plateau show similar timing and magnitudes of exhumation relative to South Africa, starting in the lowlands and shifting into the continental interior tens of millions of years later (see Methods section 'Testing broader applicability'). In Eastern Brazil (Fig. 1a), exhumation shifts from the continental margins (lowlands) during rifting and break-up—where it persists long after break-up—into the continental interior tens of millions of years later[56,57] (Extended Data Fig. 10d). The available AHe ages show a general, though imperfect, trend towards younger ages cratonward, in good agreement with model predictions (Extended Data Fig. 10c). Although more work is needed to establish spatiotemporal variations related to rifting and break-up across the continents, these first-order patterns hint at a widespread process common to cratons.

Landscape and geomorphic evolution

Rather than proposing a direct link between the rate of mantle convective removal and escarpment retreat, we suggest that a long-wavelength front of erosion migrates across the continent, tracking expected rates of convective removal. Although our geodynamic model cannot be used to directly interpret changes in surface topography, it can predict general areas of uplift and erosion over time (Fig. 2). To test whether our model is consistent with basic geomorphic principles, we thus use the well-tested landscape-evolution model Fastscape[58]. Fastscape is a 'plan-view' model that solves the stream power law (SPL) and flexure equations in 2D (*x* and *y* directions) to compute a vertical surface displacement and secondary quantities such as erosion, erosion rate and drainage area (for governing equations, see Methods). We first use this model to predict the topographic and erosional characteristics forced by a Gaussian-shaped wave of uplift that migrates laterally with a velocity of 20 km Myr^{-1} and that is characterized by a half-Gaussian width of 200 km, properties informed by simulations (Fig. 2). The model assumes an initial plateau topography of 500 m and an erodibility coefficient, K_f, of 1×10^{-5} m$^{0.2}$ year^{-1} (Methods). The model shows the predicted topography, total erosion and erosion rate at 5-Myr time steps over 50 Myr (Fig. 4a–c). Our preferred model falls in the range of plausible values for three key variables, namely, plateau height, total denudation and the final position of the drainage divide (Fig. 4 and Methods).

To explore the most probable range of K_f and initial plateau heights (h_0), we perform 120 numerical experiments of landscape evolution

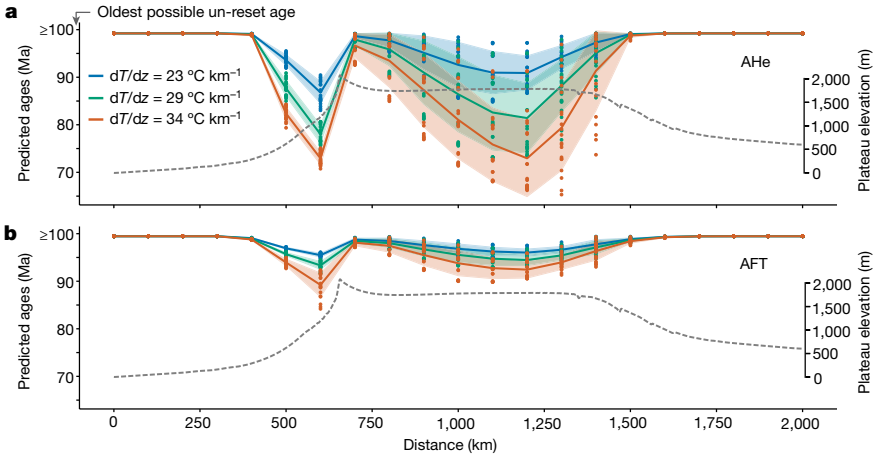

Fig. 5 | Predicted thermochronological ages in the surface-process model. Predicted ages from Fastscape for the AHe (**a**) and AFT (**b**) systems, assuming three different geothermal gradients and considering the same case as before, run for 50 Myr (that is, model 'X' in Fig. 4). Each point represents ages computed on a 21 × 21-point grid. The solid lines denote the mean (in the *y* direction) and the shaded areas correspond to the mean ± the standard deviation (in the *y* direction). For comparison with observed data in Southern Africa and Eastern Brazil, see Extended Data Figs. 9b and 10c, respectively.

(Extended Data Figs. 11 and 12) to calculate the misfit function (μ)—a mathematical function that measures the discrepancy between the modelled values of a system and the empirical observations of that system—assuming an optimal plateau height (1,650 ± 250 m), a total amount of denudation (2,750 ± 500 m) and the final position of the drainage divide (650 ± 100 km; Fig. 4d). Where the predicted values of the model fall between the assumed optimal value and uncertainty are shown in Fig. 4d, these suggest that a range of values for h_0, between 0 and 1,000 m, provide a good fit to both observational constraints and models (Fig. 4). The models confirm that, although initially shaped by mantle processes near the rift, escarpments retreat inboard of the rift and stall at a relatively early stage to become a pinned drainage divide. Nevertheless, the broad wave of uplift and denudation continues to migrate towards the craton interior (Fig. 4b,c), as is generally observed (Fig. 3a). Further, the modelled pattern of erosion across the plateau (Fig. 4b) is in good agreement with observations (Fig. 3b).

Using Fastscape to compute predicted ages for AHe and AFT (Methods), we identify two distinct regions of AHe reset ages (Fig. 5): one along the escarpment related to continuing escarpment retreat (at which the youngest ages are typically found in South Africa[18]) and one on top of the plateau, with ages becoming younger from west to east in response to the eastward propagation of the mantle forcing (Fig. 4). AFT ages exhibit either minimal or no resetting on the plateau owing to the higher closure temperature of this system (Fig. 5). Consistently, thermochronology data indicate a wider range of AHe and AFT ages near escarpments (Fig. 3a and Extended Data Figs. 9 and 10). The models help explain cases at the northeastern fringes of the Central Plateau, at which either gradual or minimal exhumation occurred during the Mesozoic[53]—sites that fall outside the main catchment of the Karoo/Orange rivers (Extended Data Fig. 4a), constraining the probable northeastern limit of erosional propagation. Generally, the main patterns observed in our model (Fig. 5) show good agreement with data from Southern Africa and Brazil, with AHe ages being predominantly younger than AFT ages (Extended Data Figs. 9 and 10). Overall, this model serves as a useful benchmark to guide future thermochronological efforts in such regions.

Deep Earth forcing of craton exhumation

Our findings show that a migrating wave of uplift (Fig. 3a–c), forced by sequential delamination of lithospheric keel, can generate a stable flat plateau even though thousands of metres of rock have been eroded (Fig. 4a–b). Estimated exhumation magnitudes from thermochronology spanning the past 180 Myr (Fig. 3b) are considered as upper-bound estimates, considering the partial preservation of Upper Cretaceous kimberlite pipes in Southern Africa[32] that may imply bedrock erosion of 1.0–1.5 km, at least locally, since that time[24]. Although our analytical models suggest a maximum likely denudation of about 1.6 km due purely to delamination, these estimates do not account for uplift related to dynamic mantle support[34], which may superpose to the vertical motion tied to convective delamination. Further, the analytical models do not consider density changes resulting from melt metasomatism in the lower lithosphere[11] nor do they consider longer-term (that is, about 10 Myr) lithospheric thinning owing to convective removal. Geodynamic models suggest that such thinning[39] can lead to extra uplift of more than 500 m.

Our model can explain the gradual eastward wave of exhumation across the Central Plateau[44], which intensified during the Late Cretaceous (100–80 Ma; Fig. 3) and is consistent with plausible topography-formation scenarios[18,46]. Notably, peak exhumation rates (Extended Data Fig. 8a) coincide with the highest frequency of kimberlite eruptions after 100 Ma (ref. 11). Collectively, our current and previous work[11] suggests that both processes are related to the sequential disruption of lithospheric keels (Figs. 2 and 5) but may operate on different timescales: kimberlite volcanism occurs rapidly, whereas uplift and denudation may (or may not) occur more slowly, reflecting slower landscape-response times that are modulated by regional differences in climatic and drainage conditions.

We infer that the overall trend in exhumation magnitude, with two prominent clusters on the plateau (Fig. 3b), is controlled by the evolution of the fluvial landscape over tens of millions of years in response to delamination of lithospheric mantle keel (Figs. 4b and 6). While alternative topography-formation scenarios propose up to 1 km of plateau uplift in the Cenozoic[18], global-scale landscape-evolution models—incorporating palaeoelevation and palaeoclimate forcings—simulate low erosion rates across the plateau during this time[46], consistent with observations[53]. Even at the Cenozoic peak, sediment volumes in the Orange Basin were approximately an order of magnitude lower than those of the Late Cretaceous[45,46], indicating much lower denudation during any late-stage plateau uplift. Although our model does not preclude a second plateau uplift phase during the Cenozoic, it favours primary topography formation during the Cretaceous. Nonetheless, prolonged low erosion rates over the Cenozoic shaped the present-day low-relief topography[43].

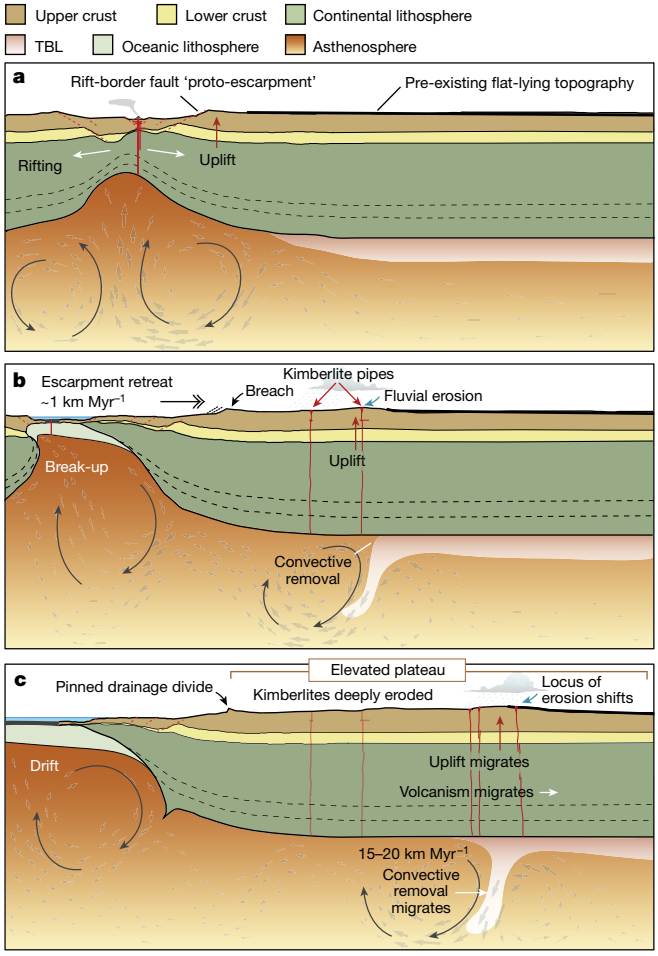

Fig. 6 | Simplified conceptual model of rifting, escarpment formation and exhumation of craton interiors. a, Rifting causes edge-driven convection in the mantle, rift-flank uplift and escarpment formation. **b**, Rayleigh–Taylor instability migrates along the lithospheric root, resulting in convective removal of the TBL of the lithospheric keel, driving kimberlite volcanism[11], isostatic uplift and denudation. **c**, Escarpment becomes a pinned drainage divide that is locally breached by the main rivers draining the plateau. Meanwhile, the convective instability continues to migrate towards the continental interior, leading to isostatic uplift, a shift in the locus of erosion and plateau formation (Fig. 4).

Surface record of continental break-up

Overall, our findings reveal a mechanistic linkage between continental rifting, escarpment formation and exhumation of craton interiors (Fig. 6), challenging the notion of 'passive' margins (supporting refs. 30,50,55). Our model identifies a common sequence of events during continental break-up, which includes: (1) rifting and escarpment formation; (2) full break-up and pinning of the escarpment; and (3) rift-driven delamination of lithospheric mantle, which sequentially migrates inboard of the rift zone (Fig. 2). Similarly, bedrock exhumation migrates sequentially, persisting for several tens of millions of years after rift cessation (Fig. 3). This exhumation, related to organized plateau growth (Fig. 4), offers a new explanation for the inferred secular exhumation of otherwise stable cratonic interiors[6], explaining their enigmatic rejuvenation long after rifting and break-up (Fig. 6). Given that continental erosion strongly influences global chemical weathering intensity and palaeoclimates, this framework offers new insights into how the deep Earth regulates climate and biosphere evolution over geological timescales.

Online content

Any methods, additional references, Nature Portfolio reporting summaries, source data, extended data, supplementary information, acknowledgements, peer review information; details of author contributions and competing interests; and statements of data and code availability are available at https://doi.org/10.1038/s41586-024-07717-1.

1. Matmon, A., Bierman, P. & Enzel, Y. Pattern and tempo of great escarpment erosion. *Geology* **30**, 1135–1138 (2002).
2. Gilchrist, A. R. & Summerfield, M. A. Differential denudation and flexural isostasy in formation of rifted-margin upwarps. *Nature* **346**, 739–742 (1990).
3. Sacek, V., Braun, J. & van der Beek, P. The influence of rifting on escarpment migration on high elevation passive continental margins. *J. Geophys. Res. Solid Earth* **117**, B04407 (2012).
4. Wang, Y. & Willett, S. D. Escarpment retreat rates derived from detrital cosmogenic nuclide concentrations. *Earth Surf. Dyn.* **9**, 1301–1322 (2021).
5. Stanley, J. R., Flowers, R. M. & Bell, D. R. Erosion patterns and mantle sources of topographic change across the southern African Plateau derived from the shallow and deep records of kimberlites. *Geochem. Geophys. Geosyst.* **16**, 3235–3256 (2015).
6. Wang, Y. et al. Secular craton evolution due to cyclic deformation of underlying dense mantle lithosphere. *Nat. Geosci.* **16**, 637–645 (2023).
7. Steckler, M. S. Uplift and extension at the Gulf of Suez: indications of induced mantle convection. *Nature* **317**, 135–139 (1985).
8. Buck, W. R. Small-scale convection induced by passive rifting: the cause for uplift of rift shoulders. *Earth Planet. Sci. Lett.* **77**, 362–372 (1986).
9. Houseman, G. A., McKenzie, D. P. & Molnar, P. Convective instability of a thickened boundary layer and its relevance for the thermal evolution of continental convergent belts. *J. Geophys. Res. Solid Earth* **86**, 6115–6132 (1981).
10. Conrad, C. P. & Molnar, P. The growth of Rayleigh–Taylor-type instabilities in the lithosphere for various rheological and density structures. *Geophys. J. Int.* **129**, 95–112 (1997).
11. Gernon, T. M. et al. Rift-induced disruption of cratonic keels drives kimberlite volcanism. *Nature* **620**, 344–350 (2023).
12. Blackburn, T. J. et al. An exhumation history of continents over billion-year time scales. *Science* **335**, 73–76 (2012).
13. Perchuk, A. L., Gerya, T. V., Zakharov, V. S. & Griffin, W. L. Building cratonic keels in Precambrian plate tectonics. *Nature* **586**, 395–401 (2020).
14. Hu, J. et al. Modification of the Western Gondwana craton by plume–lithosphere interaction. *Nat. Geosci.* **11**, 203–210 (2018).
15. Artemieva, I. M. & Vinnik, L. P. Density structure of the cratonic mantle in southern Africa: 1. Implications for dynamic topography. *Gondwana Res.* **39**, 204–216 (2016).
16. Hoggard, M. J., White, N. & Al-Attar, D. Global dynamic topography observations reveal limited influence of large-scale mantle flow. *Nat. Geosci.* **9**, 456–463 (2016).
17. Amidon, W. H., Roden-Tice, M., Anderson, A. J., McKeon, R. E. & Shuster, D. L. Late Cretaceous unroofing of the White Mountains, New Hampshire, USA: an episode of passive margin rejuvenation? *Geology* **44**, 415–418 (2016).
18. Stanley, J. R. et al. Constraining plateau uplift in southern Africa by combining thermochronology, sediment flux, topography, and landscape evolution modeling. *J. Geophys. Res. Solid Earth* **126**, e2020JB021243 (2021).
19. Neuharth, D. et al. Evolution of rift systems and their fault networks in response to surface processes. *Tectonics* **41**, e2021TC007166 (2022).
20. Braun, J. & Beaumont, C. A physical explanation of the relation between flank uplifts and the breakup unconformity at rifted continental margins. *Geology* **17**, 760–764 (1989).
21. Braun, J. A review of numerical modeling studies of passive margin escarpments leading to a new analytical expression for the rate of escarpment migration velocity. *Gondwana Res.* **53**, 209–224 (2018).
22. Spotila, J. A. et al. Origin of the Blue Ridge escarpment along the passive margin of Eastern North America. *Basin Res.* **16**, 41–63 (2004).
23. van der Beek, P., Summerfield, M. A., Braun, J., Brown, R. W. & Fleming, A. Modeling postbreakup landscape development and denudational history across the southeast African (Drakensberg Escarpment) margin. *J. Geophys. Res. Solid Earth* **107**, 2351 (2002).
24. Hanson, E. K. et al. Cretaceous erosion in central South Africa: evidence from upper-crustal xenoliths in kimberlite diatremes. *South Afr. J. Geol.* **112**, 125–140 (2009).
25. Stanley, J. R., Flowers, R. M. & Bell, D. R. Kimberlite (U-Th)/He dating links surface erosion with lithospheric heating, thinning, and metasomatism in the southern African Plateau. *Geology* **41**, 1243–1246 (2013).
26. Van Ranst, G., Pedrosa-Soares, A. C., Novo, T., Vermeesch, P. & De Grave, J. New insights from low-temperature thermochronology into the tectonic and geomorphologic evolution of the south-eastern Brazilian highlands and passive margin. *Geosci. Front.* **11**, 303–324 (2020).
27. Turner, J. P., Green, P. F., Holford, S. P. & Lawrence, S. R. Thermal history of the Rio Muni (West Africa)–NE Brazil margins during continental breakup. *Earth Planet. Sci. Lett.* **270**, 354–367 (2008).
28. Japsen, P., Chalmers, J. A., Green, P. F. & Bonow, J. M. Elevated, passive continental margins: not rift shoulders, but expressions of episodic, post-rift burial and exhumation. *Glob. Planet. Change* **90–91**, 73–86 (2012).
29. Wildman, M. et al. The chronology and tectonic style of landscape evolution along the elevated Atlantic continental margin of South Africa resolved by joint apatite fission track and (U-Th-Sm)/He thermochronology. *Tectonics* **35**, 511–545 (2016).
30. Cogné, N., Gallagher, K., Cobbold, P. R., Riccomini, C. & Gautheron, C. Post-breakup tectonics in southeast Brazil from thermochronological data and combined inverse-forward thermal history modeling. *J. Geophys. Res. Solid Earth* **117**, B11413 (2012).

31. Brown, R. W., Summerfield, M. A. & Gleadow, A. J. W. Denudational history along a transect across the Drakensberg Escarpment of southern Africa derived from apatite fission track thermochronology. *J. Geophys. Res. Solid Earth* **107**, 2350 (2002).
32. Braun, J., Guillocheau, F., Robin, C., Baby, G. & Jelsma, H. Rapid erosion of the Southern African Plateau as it climbs over a mantle superswell. *J. Geophys. Res. Solid Earth* **119**, 6093–6112 (2014).
33. Jones, S. M., Lovell, B. & Crosby, A. G. Comparison of modern and geological observations of dynamic support from mantle convection. *J. Geol. Soc.* **169**, 745–758 (2012).
34. Jones, A. G., Afonso, J. C. & Fullea, J. Geochemical and geophysical constrains on the dynamic topography of the Southern African Plateau. *Geochem. Geophys. Geosyst.* **18**, 3556–3575 (2017).
35. King, S. D. & Ritsema, J. African hot spot volcanism: small-scale convection in the upper mantle beneath cratons. *Science* **290**, 1137–1140 (2000).
36. Ebinger, C. J., Jackson, J. A., Foster, A. N. & Hayward, N. J. Extensional basin geometry and the elastic lithosphere. *Philos. Trans. R. Soc. Lond. A Math. Phys. Eng. Sci.* **357**, 741–765 (1999).
37. Jeanniot, L. & Buiter, S. J. H. A quantitative analysis of transtensional margin width. *Earth Planet. Sci. Lett.* **491**, 95–108 (2018).
38. Braun, J., Robert, X. & Simon-Labric, T. Eroding dynamic topography. *Geophys. Res. Lett.* **40**, 1494–1499 (2013).
39. van Wijk, J. W. et al. Small-scale convection at the edge of the Colorado Plateau: implications for topography, magmatism, and evolution of Proterozoic lithosphere. *Geology* **38**, 611–614 (2010).
40. Griffin, W. L., O'Reilly, S. Y., Natapov, L. M. & Ryan, C. G. The evolution of lithospheric mantle beneath the Kalahari Craton and its margins. *Lithos* **71**, 215–241 (2003).
41. Pasyanos, M. E., Masters, T. G., Laske, G. & Ma, Z. LITHO1.0: an updated crust and lithospheric model of the Earth. *J. Geophys. Res. Solid Earth* **119**, 2153–2173 (2014).
42. Afonso, J. C., Salajegheh, F., Szwillus, W., Ebbing, J. & Gaina, C. A global reference model of the lithosphere and upper mantle from joint inversion and analysis of multiple data sets. *Geophys. J. Int.* **217**, 1602–1628 (2019).
43. Kounov, A., Viola, G., de Wit, M. J. & Andreoli, M. A Mid Cretaceous paleo-Karoo River valley across the Knersvlakte plain (northwestern coast of South Africa): evidence from apatite fission-track analysis. *South Afr. J. Geol.* **111**, 409–420 (2008).
44. Stanley, J. R. & Flowers, R. M. Mesozoic denudation history of the lower Orange River and eastward migration of erosion across the southern African Plateau. *Lithosphere* **12**, 74–87 (2020).
45. Baby, G. et al. Post-rift stratigraphic evolution of the Atlantic margin of Namibia and South Africa: implications for the vertical movements of the margin and the uplift history of the South African Plateau. *Mar. Pet. Geol.* **97**, 169–191 (2018).
46. Salles, T. et al. Hundred million years of landscape dynamics from catchment to global scale. *Science* **379**, 918–923 (2023).
47. Bell, D. R., Schmitz, M. D. & Janney, P. E. Mesozoic thermal evolution of the southern African mantle lithosphere. *Lithos* **71**, 273–287 (2003).
48. Tinker, J., de Wit, M. & Brown, R. Mesozoic exhumation of the southern Cape, South Africa, quantified using apatite fission track thermochronology. *Tectonophysics* **455**, 77–93 (2008).
49. Flowers, R. M. & Schoene, B. (U-Th)/He thermochronometry constraints on unroofing of the eastern Kaapvaal craton and significance for uplift of the southern African Plateau. *Geology* **38**, 827–830 (2010).
50. Wildman, M. et al. Post break-up tectonic inversion across the southwestern cape of South Africa: new insights from apatite and zircon fission track thermochronometry. *Tectonophysics* **654**, 30–55 (2015).
51. Ketcham, R. A. Forward and inverse modeling of low-temperature thermochronometry data. *Rev. Mineral. Geochem.* **58**, 275–314 (2005).
52. Molnar, P., England, P. C. & Jones, C. H. Mantle dynamics, isostasy, and the support of high terrain. *J. Geophys. Res. Solid Earth* **120**, 1932–1957 (2015).
53. Wildman, M. et al. Contrasting Mesozoic evolution across the boundary between on and off craton regions of the South African plateau inferred from apatite fission track and (U-Th-Sm)/He thermochronology. *J. Geophys. Res. Solid Earth* **122**, 1517–1547 (2017).
54. Brune, S., Williams, S. E., Butterworth, N. P. & Müller, R. D. Abrupt plate accelerations shape rifted continental margins. *Nature* **536**, 201–204 (2016).
55. Green, P. F., Duddy, I. R., Japsen, P., Bonow, J. M. & Malan, J. A. Post-breakup burial and exhumation of the southern margin of Africa. *Basin Res.* **29**, 96–127 (2017).
56. Harman, R., Gallagher, K., Brown, R., Raza, A. & Bizzi, L. Accelerated denudation and tectonic/geomorphic reactivation of the cratons of northeastern Brazil during the Late Cretaceous. *J. Geophys. Res. Solid Earth* **103**, 27091–27105 (1998).
57. Fonseca, A. C. L. et al. Differential Phanerozoic evolution of cratonic and non-cratonic lithosphere from a thermochronological perspective: São Francisco Craton and marginal orogens (Brazil). *Gondwana Res.* **93**, 106–126 (2021).
58. Willett, S. D. & Braun, J. A very efficient *O*(*n*), implicit and parallel method to solve the stream power equation governing fluvial incision and landscape evolution. *Geomorphology* **180**, 170–179 (2013).
59. Müller, R. D. et al. GPlates: building a virtual Earth through deep time. *Geochem. Geophys. Geosyst.* **19**, 2243–2261 (2018).